Chinese Chemical Letters 32 (2021) 3653–3664

Contents lists available at ScienceDirect

Chinese Chemical Letters

journal homepage: www.elsevier.com/locate/cclet

Review

Long-wavelength (red to near-infrared) emissive carbon dots: Key factors for synthesis, fluorescence mechanism, and applications in biosensing and cancer theranostics

Aman Lv[a,b], Qiao Chen[b], Chen Zhao[b], Si Li[c], Shan Sun[b,c,*], Junping Dong[a], Zhongjun Li[d], Hengwei Lin[c,*]

[a] College of Science, Shanghai University, Shanghai 200444, China
[b] Cixi Institute of Biomedical Engineering, Chinese Academy of Science (CAS) Key Laboratory of Magnetic Materials and Devices & Zhejiang Engineering Research Center for Biomedical Materials, Ningbo Institute of Materials Technology and Engineering, CAS, Ningbo 315201, China
[c] International Joint Research Center for Photo-responsive Molecules and Materials, School of Chemical and Material Engineering, Jiangnan University, Wuxi 214122, China
[d] College of Chemistry and Molecular Engineering, Zhengzhou University, Zhengzhou 450001, China

ARTICLE INFO

Article history:
Received 26 March 2021
Revised 31 May 2021
Accepted 7 June 2021
Available online 16 June 2021

Keywords:
Long-wavelength emission
Carbon dots
Fluorescence mechanism
Sensing
Cancer theranostics

ABSTRACT

Carbon dots (CDs), as a new member of carbon nanostructures, have been widely applied in extensive fields due to their exceptional physicochemical properties. While, the emissions of most reported CDs are located in the blue to green range under the excitation of ultraviolet or blue light, which severely limits their practical applications, especially in photovoltaic and biological fields. Studies that focused on synthesizing CDs with long-wavelength (red to near-infrared) emission/excitation features (simply named L-w CDs) and exploring their potential applications have been frequently reported in recent years. In this review, we analyzed the key influence factors for the synthesis of CDs with long wavelength and multicolor (containing long wavelength) emissive properties, discussed possible fluorescence mechanism, and summarized their applications in sensing and cancer theranostics. Finally, the existing challenges and potential opportunities of L-w CDs are presented.

1. Introduction

Carbon dots (CDs), also being called carbon nanodots (CNDs), carbon quantum dots (CQDs), graphene quantum dots (GQDs), or carbonized polymer dots (CPDs), are generally defined as a zero-dimensional (0D) luminescent carbon nanostructure with average size less than 20 nm [1-3]. Since their discovery in 2004 [4], CDs have attracted much attention due to their specific optical properties, superior biocompatibility, economic preparation, environment-friendliness, and excellent photostability, *etc.* Over the past decade, numerous convenient and reproducible synthesis methods of CDs were developed, among which the hydrothermal, solvothermal, and microwave-assisted one-step approaches are commonly used [5-9]. CDs are considered to have a conjugated structure that consists of a graphitized sp^2 carbon core and an amorphous shell functionalized with amino, carboxyl, and hydroxy groups [10-13]. Owing to the special structure and features, CDs exhibit many superiorities, such as tunable optical properties, favorable water dispersibility, convenient surface functionalization, and most attractively the hyperthermia and reactive oxygen species (ROS) generation capability triggered by physicochemical stimuli [14-17]. Thus, CDs are regarded as promising candidates for various applications, including sensors, optoelectronic devices, photocatalysis, anti-counterfeiting, and biomedical use [18-23]. However, the fluorescence (FL) emission of most reported CDs were located in blue to green range with the excitation of ultraviolet (UV) or blue light [24,25], which severely restricted their applications, especially in photovoltaic and biological fields. It is well known that red phosphor is one of the indispensable components for the fabrication of full-color and white light-emitting diodes [26-28]. Likewise, the FL signal among blue to green range can be interfered with autofluorescence of biological tissue; besides, normal matrix might suffer from serious photodamage induced by UV light irradiation [29,30]. Overall, the development of long-wavelength (*i.e.*, red to near-infrared (NIR)) emissive/excitative CDs

* Corresponding authors.
E-mail addresses: sunshan@nimte.ac.cn (S. Sun), linhengwei@jiangnan.edu.cn (H. Lin).

https://doi.org/10.1016/j.cclet.2021.06.020
1001-8417/

(simply named L-w CDs) is quite necessary. So far, numerous studies have been conducted and great progress has been achieved in the research of L-w CDs. Except for the above-mentioned superiorities, L-w CDs present additional advantages, including broad absorption band tail up to NIR region, FL emission with multi-photon excitation, and favorable photoacoustic (PA) responsiveness [31,32], which make them a very attractive photoluminescence nanomaterial.

Based on the unique features and great application potential of L-w CDs, this review will summarize the existing researches and emerging advances of such CDs from a specific perspective to guide their synthesis with desirable optical properties. Brief introductions of representative works were presented in Table 1 for outlining this research field. Specifically, the crucial factors for the synthesis of L-w CDs are primarily reviewed, including precursors, reaction conditions, and post-modification routes. In particularly, we will focus on their FL mechanism from the viewpoints of size effect, surface state, heteroatom doping, and solvatochromic shift. Furthermore, the applications of L-w CDs, especially in sensing and cancer theranostics are summarized to outlook their potential values, for example as highly sensitive detection probes, smart drug carriers, multifunctional imaging, and therapeutic agents. Finally, the current challenges and future perspectives of L-w CDs will be discussed, which may be helpful for their development in the future.

2. Key influential factors for the synthesis of L-w CDs

Numerous synthesis methods of CDs have been reported since their discovery in 2004 [4], which were generally divided into two categories: top-down and bottom-up approaches [14,21,33], including laser ablation [34,35], exfoliation [36,37], hydrothermal and solvothermal synthesis [38,39], and microwave-assisted pyrolysis [40,41], *etc.* Although great efforts have been made to prepare CDs with L-w absorption and emission properties, the tailoring of their emission wavelength into the red and NIR region is still impeded by the limited understanding of the relationship between CDs' structure and their optical performance. In this section, we intend to clarify the key factors for the synthesis of L-w CDs rather than focusing on the synthesis methods, which mainly include precursors [39,42-47], reaction conditions [48-51], and post-modification routes [7,52,53].

2.1. Precursors

Precursors that selected for the synthesis of L-w CDs usually contain appropriate aromatic structures and/or various heteroatoms, which can narrow the energy gap *via* the production of large sp^2 domains as well as the introduction of new energy levels, consequently causing redshifts of their FL wavelength. Small molecules that used as synthetic precursors (*e.g.*, aromatic molecules and dye molecules) and biomass are discussed as follows.

Our group has performed notable research in the synthesis of L-w CDs using small molecules as precursors. One of the typical examples is the facile synthesis of high efficient red-emissive CDs (R-CDs) through microwave-mediated pyrolysis of citric acid in formamide (Fig. 1a) [39]. The as-prepared R-CDs exhibited pure red emission ($\lambda_{em}{}^{max}$ = 640 nm) with a high quantum yield (QY) of 22.9%. Notably, the L-w emission feature disappeared if formamide was replaced by other solvents such as water, ethanol, and dimethylformamide (DMF), demonstrating the critical role of formamide in the successful synthesis of R-CDs. Later, we prepared CDs with NIR FL emission *via* microwave-assisted heating of glutathione formamide solution (Fig. 1b) [42]. The maximum NIR emission wavelength of CDs located at around 683 nm with a narrow emission band and a QY of 16.8%.

Wang's group used polythiophene derivatives as the carbon source to prepare functional CDs, which not only displayed red emission (maximum wavelength at around 640 nm) but also held photo-mediated therapeutic potential (Fig. 1c) [43]. This work opened a door for designing L-w CDs with theranostic functions. More recently, Fan's group utilized dye molecule 1,4,5,8-tetraminoanthraquinone (TAAQ) and citric acid to synthesize NIR emissive CDs, which showed an excitation-independent emission peak near 700 nm [44]. Zheng and co-workers reported a strategy to prepare CDs with both NIR absorption and emission features using cyanine dye molecule as precursor (Fig. 1d) [45]. In contrast with the hydrophobic cyanine dyes, the as-prepared CDs displayed excellent water solubility and enhanced photostability, which provide a valuable method for converting hydrophobic dye molecules into hydrophilic functional materials while preserving their optical properties.

Interestingly, biomass is also considered as potential candidates for the preparation of L-w CDs. For example, Li's group synthesized NIR-light emissive CDs from spinach using a one-pot solvothermal method (Fig. 1e) [47]. The NIR CDs can be well dispersed in water with a typical emission maximum at 680 nm. Besides, Yang's group utilized Taxus leaves as a carbon source to prepare CDs with a deep-red emission at ~673 nm and an extreme-narrow full width half maximum (FWHM) of ~20 nm (Fig. 1f) [46]. The deep-red emission of biomass-derived CDs might be attributed to the presence of porphin structures in the chlorophyll of green leaves.

2.2. Reaction conditions

Reaction conditions play a significant role in tuning the optical properties of CDs. Clarifying the relationship between redshifted emission of CDs and synthetic conditions including temperature, time, solvent, and reactants ratio could deepen the understanding for regulating FL properties of CDs.

As discussed in our previous work, using the same approach but with relatively low temperature and short reaction time, only blue-light emissive CDs were obtained instead of the full-color emissive CDs [48]. Later, Huang and co-workers also illustrated a close connection between the reaction conditions (specifically the temperature and time) and optical properties [49]. They found that the L-w shift of FL emission from ~570 nm to 700 nm was mainly caused by the structural evolution during the hydrothermal treatment. Qu's group provided solid evidence for the solvent-affected emissive behavior of CDs that originated from the same precursors [50]. It has been observed that compared to protic solvents (*e.g.*, water), the aprotic solvents (*e.g., N,N*-dimethylformamide, DMF) tend to induce higher extent of dehydration and carbonization of carbon source. Thus, full-color emissive CDs with FL range covering blue to red region can be successfully synthesized by adjusting the type and ratio of solvents. Wu's group proposed an acid-assisted engineering strategy for preparing a series of CDs [51]. By using different acid reagents and adjusting the mass ratio of *o*-phenylenediamine and acid, the FL emission of CDs could be flexibly regulated from blue to red region. Most recently, multi-color emissive carbon dots were synthesis by Lu's group in a single reaction system, from which the FL variation from blue to NIR was proved to depend on the adjustment of pH and temperature [54]. Taken together, it can be inferred that the emission of CDs is strongly depended on the reaction conditions.

2.3. Post-modification methods

Apart from the above-mentioned factors that affect the synthesis of L-w CDs, post-modification also has a direct effect on

Table 1
Brief introductions of representative works in the research field of L-w CDs.

Precursors	Synthesis methods	Em_{max} (nm)	QY (%)	Applications	Ref.
Waste expanded polystyrene, dichloromethane	Solvothermal	470, 530, 630	5.2, 3.4, 3.1	White/multi-color light-emitting diodes	[28]
Citric acid, formamide	Microwave-mediated	640	22.9	Multifunctional theranostic	[39]
Glutathione, formamide	Microwave-mediated	683	16.8	Bioimaging	[42]
Polythiophene phenylpropionic acid	Oxidative polymerization	640	2.3	Fluorescent, photoacoustic, and thermal theranostics	[43]
1,4,5,8-Tetraminoanthraquinone, citric acid	Hydrothermal	700	6.8–10.7	tumor theranostics	[44]
Hydrophobic cyanine dye	Solvothermal	820	_	Imaging and photothermal cancer therapy	[45]
Taxus leaves	Solvothermal	673	59	Deep tissue bioimaging	[46]
Spinach	Solvothermal	680	_	Bio-imaging	[47]
Citric acid, urea	Solvothermal	638	8	CDot-based LEDs	[50]
o-Phenylenediamine	Solvothermal	400–700	25–72	White light-emitting diodes (WLEDs)	[51]
Graphite nanoparticles	Mechanical exfoliation	~450–630	9.7–15.4	Optoelectronic devices	[52]
p-Phenylenediamine	Hydrothermal	352, 527, 610	20.3, 35.2 18.9	Bioimaging *in vitro* and *in vivo*	[53]
L-/D-Tryptophan, *o*-phenylenediamine	Solvothermal	441, 546, 604	53.62(water), 31.65(ethanol), 46.38 (ethanol)	_	[54]
o-, *m*-, *p*-Phenylenediamines	Solvothermal	435–604	4.8–26.1	Cellular imaging	[56]
Urea and *p*-phenylenediamine	Hydrothermal	440–625	8.53–35.14	Image cells and image mice	[62]
1,2,4,5-Benzenetetracarboxylic acid, 2,7-diaminofluorene	Solvothermal	475–605	0.1–0.26	_	[63]
Citric acid	Solvothermal	600–800	9.8	*In vivo* NIR imaging	[64]
Polythiophene, diphenyl diselenide	Hydrothermal	~731,820	~0.2	Biomedical application, cancer diagnosis and treatment	[66]
2,5-Diaminobenzenesulfonic acid, 4-aminophenylboronic acid hydrochloride	Hydrothermal	600	5.44	Colorimetric and fluorescent dual mode detection of Fe^{3+} ions	[67]
p-Phenylenediamine	Solvothermal	540–614	20.6–71.8	_	[69]
Citric acid, urea	Solvothermal	760	10	*In vivo* NIR fluorescence imaging	[71]
Citric acid formamide solution	Microwave-mediated	466, 555, 637	11.9, 16.7, 26.2	Multicolor cellular imaging and multidimensional sensing	[72]
Aminosalicylic acid	Solvothermal	416–646	5.8–16.4	Cell imaging and sensitive detection of Fe^{3+} in living cells	[90]
Citric acid, neutral red	Hydrothermal	632–648	8.9 −12.1	Sensing of Pt^{2+}, Au^{3+}, and $Pd^{2+}$and their bioapplications *in vitro* and *in vivo*	[92]
Citric acid, formamide	Microwave reaction	640	22.9	Detection and discrimination of phosphate anions	[93]
Citric acid, formamide	Microwave reaction	640	19.5	Peroxynitrite ($ONOO^-$) detection	[94]
o-Phenylenediamine, phosphoric acid	Hydrothermal	440–624	_	Ratiometric detection of intracellular lysine and pH	[95]
Citric acid, formamide	Microwave reaction	640	26.2	Detection and differentiation of antibiotics	[96]
Glutathione, formamide	Solvothermal	680	16.4	Determination of carcinoembryonic antigen in pleural effusion	[97]
Sugar cane bagasse, concentrated phosphoric acid, concentrated sulfuric acid	One-step carbonization	575–630	_	Selective probing of gaseous ammonia	[98]
o-Phenylenediamine, dopamine	Hydrothermal	685	33.96	Cellular sensing and light-emitting diodes	[99]
Pulp-free lemon juice, formamide	Solvothermal	704	31	Bioimaging both *in vitro* and *in vivo*	[107]
Dopamine, *o*-phenylenediamine	Hydrothermal	710	26.28	*In vivo* bioimaging and red LEDs	[108]
10,15,20-Tetrakis(4-aminophenyl)porphyrin, citric acid	Solvothermal	750 (pH 7.0), 678 (pH 7.4)	8.54	Fluorescence and PA dual-modality imaging-guided photodynamic therapy	[112]
Watermelon juice	Solvothermal	925	0.4	*In vivo* renal-excreted optical imaging and photothermal therapy	[113]
Citric acid, polyethyleneimine, formamide	Solvothermal	635	_	Fluorescence imaging and synergistic cancer therapy	[115]
Polythiophene derivatives	Hydrothermal	680	_	Bioimaging and photodynamic	[116]
Manganese(II) phthalocyanine (Mn-Pc)	Solvothermal	745	_	Bimodal imaging and enhanced photodynamic therapy	[117]
Pheophytin, *N*,*N*-dimethylformamide	Microwave synthesis	680	_	Bioimaging and photodynamic therapy	[118]

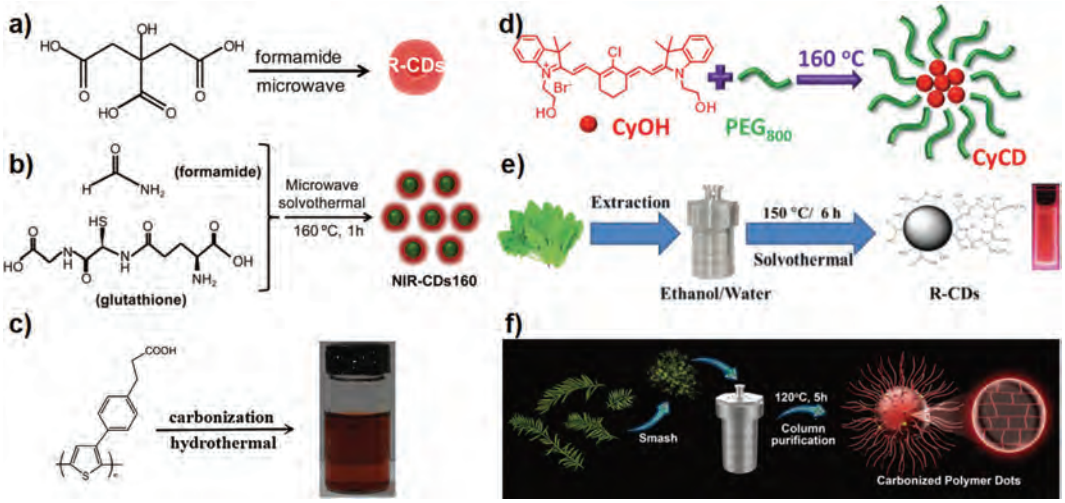

Fig. 1. (a) Illustration of the synthesis of red emissive CDs. Reproduced with permission [39]. Copyright 2016, American Chemical Society. (b) Illustration of the fabrication of NIR emissive CDs. Reproduced with permission [42]. Copyright 2016, Royal Society of Chemistry. (c) Synthetic route of polythiophene derivatives-based CDs. Reproduced with permission [43]. Copyright 2015, Wiley Publishing Group. (d) Synthetic route of CyCDs. Reproduced with permission [45]. Copyright 2016, American Chemical Society. (e) Illustration of the preparation of CDs from spinach. Reproduced with permission [47]. Copyright 2017, Royal Society of Chemistry. (f) Illustration of the synthesis of CDs from taxus leaves. Reproduced with permission [46]. Copyright 2020, Wiley Publishing Group.

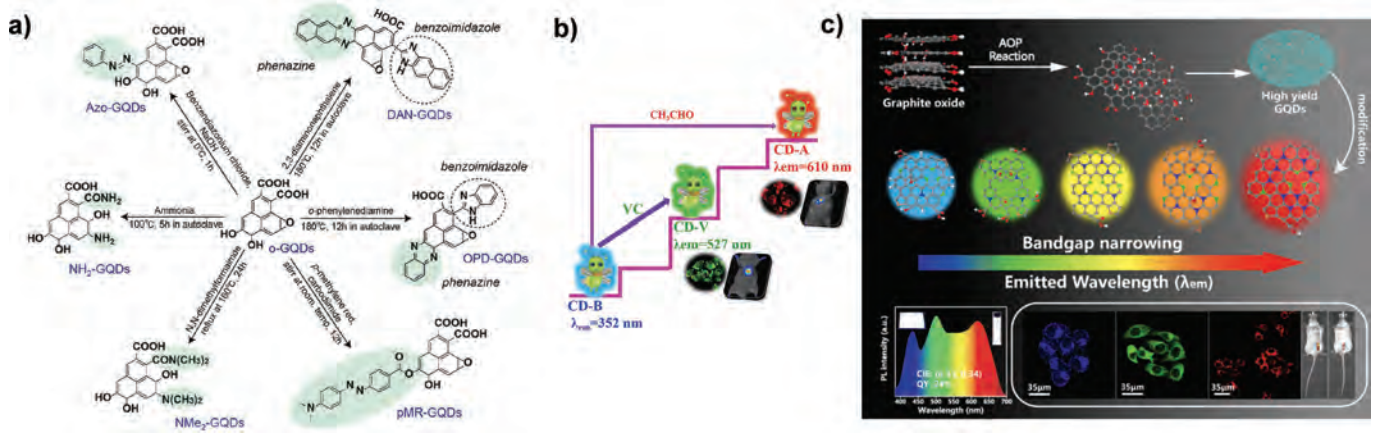

Fig. 2. (a) Synthetic scheme of different nitrogenous functionalized GQDs. Reproduced with permission [52]. Copyright 2016, Wiley Publishing Group. (b) Post modification of CD-B with Vitamin C and acetaldehyde and their applications. Reproduced with permission [53]. Copyright 2019, Royal Society of Chemistry. (c) Synthetic route of GQDs with various FL emissive features and their applications. Reproduced with permission [7]. Copyright 2020, Elsevier.

their optical properties. Tetsuka's group shifted the FL emission of GQDs from blue to red region *via* post-modification of various nitrogen-containing chemical groups (Fig. 2a) [52]. Based on the theoretical calculation and experimental results, the narrowed energy gap between the lowest unoccupied molecular orbital (LUMO) and highest occupied molecular orbital (HOMO) of GQDs induced by the nitrogenous functionalization was primarily responsible for the redshift of their FL emissions. It is noteworthy that nucleophilic substitution and dehydration reactions employed in this work could be effectively applied for the surface modification of GQDs. Besides, Xie's group reported that after reacting with vitamin C and acetaldehyde, the FL emission of as-synthesized CDs (CD-B) was tuned from blue to L-w range (Fig. 2b) [53]. Specifically, the redshifted emission maxima of CD-B can be ascribed to the introducing of sub-fluorophores such as carbonyl and C=N groups, verifying the feasibility of using post modification strategy to regulate the optical properties of CDs. Lyu and co-workers firstly reported the gram-scale preparation of well-crystalline GQDs under mild thermal-driven oxidation condition [7]. Subsequently, post-modification was applied to regulate the FL behavior of GQDs using various nitrogenous chemical molecules, which doped the graphitic nitrogen to the carbon framework and strengthened the π-conjugation, thereby the redshift of FL emission was achieved (Fig. 2c).

These results demonstrated that the regulation of optical properties of CDs can be realized *via* the selection of precursor, reaction condition, and post-modification.

3. FL mechanism of CDs

Understanding the FL mechanism is the cornerstone to obtain desirable CDs with specific optical characteristics. Although it is still difficult to elucidate the exact FL mechanism of L-w CDs, several reasonable explanations have been proposed to deepen the comprehension of FL origins, such as size effects [55-58], surface state emission [42,59-63], heteroatom doping [21,64-67], and solvatochromic shift [68-71], which are discussed in the following subsections.

3.1. Size effects

Similar with the traditional semiconductor quantum dots, the FL properties of CDs could be regulated *via* size changing. Typically, CDs exhibit L-w shifted emission along with the increase of parti-

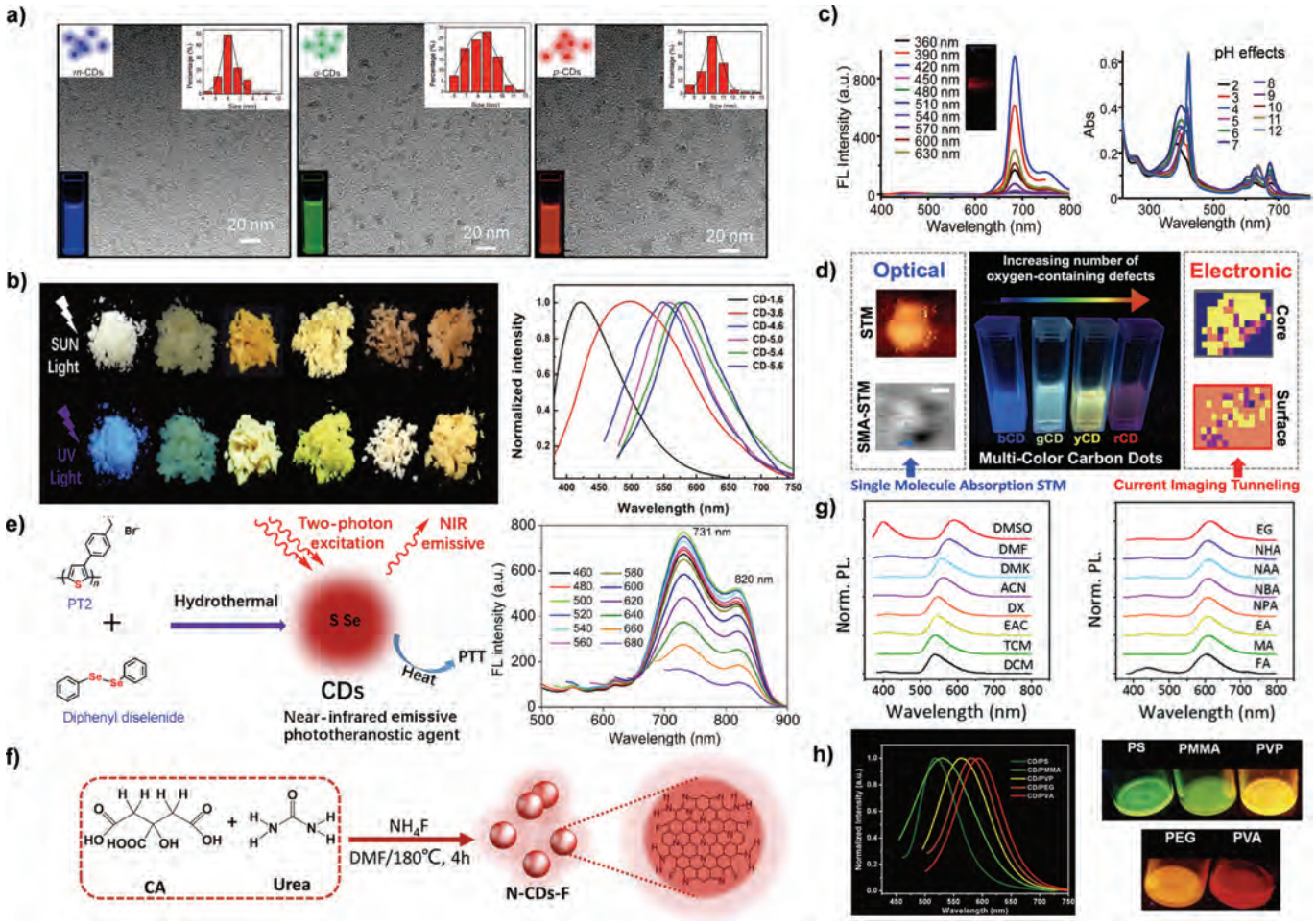

Fig. 3. (a) TEM images and size distribution of *m*-CDs, *o*-CDs, and *p*-CDs. Reproduced with permission [56]. Copyright 2015, Wiley Publishing Group. (b) Digital photos of six kinds of CDs with different particle size under daylight and UV light and corresponding normalized FL spectra. Reproduced with permission [58]. Copyright 2019, Wiley Publishing Group. (c) FL spectra of NIR CDs and their absorption spectra at various pH values. Reproduced with permission [42]. Copyright 2016, Royal Society of Chemistry. (d) Photographs of CDs with increasing number of oxygen-contained defects at excited status. Reproduced with permission [63]. Copyright 2020, American Chemical Society. (e) Synthesis and FL mechanism of S, Se-codoped CDs. Reproduced with permission [66]. Copyright 2017, Springer. (f) Schematic illustration of the synthesis of N-CDs-F. Reproduced with permission [31]. Copyright 2020, Wiley Publishing Group. (g) Normalized FL spectra in aprotic and protic solvents. Reproduced with permission [69]. Copyright 2017, Royal Society of Chemistry. (h) Normalized FL spectra of CDs embedded in different polymer films and corresponding photographs of these films at excited status. Reproduced with permission [70]. Copyright 2017, Elsevier.

cle size, which is primarily ascribed to the narrowing energy gap of sp^2-carbon-constructed core [72]. In 2015, our group proposed a facile method for the preparation of red, green, and blue photoluminescent CDs with the excitation of single UV light. The chemical composition and surface functional groups of these CDs were similar, while their average size changed from 6.0 nm of blue-CDs, 8.2 nm of green-CDs, to 10.0 nm of red-CDs (Fig. 3a), which indicated that the particle size might be responsible for the redshift of emission wavelength [56].

Ke and co-workers synthesized a series of GQD/graphene oxide (GQDs/GO) composites with the emission wavelength ranged from blue to red region [57]. It can be observed that the redshift of FL wavelength was accompanied with the size increase of GQDs/GO, which essentially attributed to the quantum confinement effect. Notably, GQDs produced from coal [73], carbon fibers [74], and carbon black [75] displayed similar size-dependent emission properties. Subsequently, Qu's group prepared full-color emissive CDs from the same reactants and revealed the hidden mechanism that the particle size increasing was accompanied by the sp^2-domains expanding and L-w absorption/emission bands shifting, which resulted from the different extents of dehydration and carbonization of precursors [50]. Moreover, Zhu *et al.* also verified the size-dependent FL phenomena of CDs at solid state [58]. As illustrated in Fig. 3b, the emission color of six kinds of CDs varies with the particle size. This size-dependent redshifted FL emission feature is primarily attributed to the increased π-conjugated domains of CDs [76-78].

3.2. Surface state emission

In addition to the size effects, the surface states, such as surface chemical composition and functional groups, are regarded as another prominent factor in affecting the emission behavior of CDs [59,60]. Specifically, surface state emission of CDs is generated *via* the recombination of electrons and holes, which is closely associated with π-electron conjugation and surface chemistry [79]. Thus, the created sub-levels of surface state might take the responsibility for the L-w shifted emission of CDs [2]. Our group has developed NIR emissive CDs (NIR-CDs) that displayed excitation-independent but pH-dependent emission properties (Fig. 3c), suggesting the surface state-governed emission mechanism [42]. Subsequently, we prepared CDs with FL emission extends to the NIR region and a high QY of 22.0% using tartaric acid (TA) and *o*-phenylenediamine as precursors [61]. Notably, FL intensity of CDs usually decreased with the increase of their surface oxidation degree, indicating a surface state-dependent FL nature.

Further, Xiong's group successfully obtained a series of CDs with tunable FL emission and high QYs *via* separation process based on silica gel column chromatography [62]. These CDs have similar particle size and graphitic structure, but the extent of surface oxidation and carboxyl content gradually increased along with the redshift of their FL emission. Therefore, the surface state is speculated to be a predominant influential factor on the FL tunability of CDs. Along with the increase of surface oxidation, the energy gap between LUMO and HOMO of CDs is reduced, leading to a redshift of the FL emission maxima [60]. It is well known that post-modification is a common route to improve the FL QY of CDs [34,80]. This strategy has also been used to modulate the optical properties of CDs through simple reactions with vitamin C and acetaldehyde by Zheng *et al.* [53]. The details have been discussed in Section 2.3. To date, the relationship between FL and the oxidized surface defects of CDs is still unclear. However, Gruebele's group provided direct evidence to explain the FL mechanism using scanning tunneling microscopy (STM). From the images of individual CDs at sub-particle resolution (Fig. 3d), it could be learnt that the increase of oxidation effects of CDs leads to a red-shifted emission [63].

3.3. Heteroatom doping

Heteroatom doping is an effective strategy to regulate the chemical composition and optical properties of CDs due to the generation of π-type or n-type carriers [21]. Thus, the introduction of atomic impurities might be a possible cause for the L-w shift of CDs emission. Due to the doping process and similar atomic size of C and N atoms, doping N atoms in the form of graphitic, pyridinic, and amino N is a widely-adopted approach to induce the FL redshift of CDs. In an earlier study, we established that the content of N plays a vital role in controlling the optical properties of CDs [56]. Inspired by this result, we proposed a facile strategy to prepare N-doped CDs with intense yellow emissive capacity, further demonstrating the feasibility of N-doping in tuning FL of CDs [65]. Furthermore, Kateřina Holá and co-workers also confirmed that the FL shift of CDs from blue to red region was mainly controlled by the doping of graphitic nitrogen in which mid gap states were generated [81].

Other dopants like sulfur (S) [82], selenium (Se) [66], boron (B) [67], and fluorine (F) [31] were also used to shift the emission of CDs into L-w region. For example, Lan and co-workers synthesized S, Se co-doped CDs with excitation-independent NIR emissive feature under both one- and two-photon excitation modes (Fig. 3e) [66]. The bandgap opening induced by the doping of heavy atoms into the graphitic lattices was considered to be a possible reason for the NIR emission [83,84]. Another kind of B, N, S co-doped CDs (BNS-CDs) was prepared by Ren's group [67]. Since the optical features of BNS-CDs was significantly influenced by the reagent ratio, elemental doping is regarded as a key factor to govern their emission behavior. Interestingly, distinct optical variations stem from different dopants. Specifically, the enhanced FL intensity might be induced by the doping of N, B, and S, which could weaken the nonradiative recombination through the increase of surface defects [85]. However, N coming from 4-aminophenylboronic acid might be responsible for L-w shifted emission due to its capability of narrowing bandgap [86]. Among these dopants, F holds great potential to reduce the energy gap between LUMO and HOMO due to its strong electron-withdraw ability, which leads to the redshift of both excitation and emission wavelengths [87,88] .Based on these facts, Jiang and co-workers designed F- and N-doped CDs by using ammonium fluoride (NH_4F), which exhibited the characteristics of UV-vis-NIR full-spectra responsiveness and multiphoton excitation up-conversion FL emission (Fig. 3f) [64]. Further, they proposed a reliable mechanism based on the inter/intra-dot hydrogen bonds existing in N-H···F that could expand the conjugated sp^2 domains, which not only decreased the HOMO-LUMO energy level but also enhanced the cross section of multiphoton absorption.

3.4. Solvatochromic shift

Apart from the structure-related luminescence mechanisms of CDs, solvent can also be used to control the luminescence of CDs. Specifically, solvatochromic shift, which implies the solvent relaxation or dipolar rearrangement occurring in the band edge, leads to a distinguished redshift of FL emission [68]. Based on Lippert-Mataga theory, redshift of FL emission is commonly induced by higher polarity of solvents [89].

Zhang and co-workers reported that the FL variation trend of CDs was different among aprotic and protic solvents (Fig. 3g) [69], which was primarily attributed to the hydrogen bond interactions between solvent molecules and CDs. Moreover, Yu's group designed excitation-independent CDs that displayed varied emission behavior when dispersed CDs in different solvents [70]. According to the effect of solvatochromic shift, CDs were further embedded in various kinds of polymer matrices to prepared CD films, which also exhibited multicolor FL from green to red region (Fig. 3h). The solvent dependent optical properties were also demonstrated by Li and co-workers, which showed that the absorption and FL emission spectra, and the QY were different if the CDs were dispersed in water or aprotic polar solvents [71]. The electron-acceptor groups of organic solvent enable them to link with the surface functional groups of CDs, leading to the variation of optical band gap and the enhancement of electron transition.

Overall, L-w emission originates from the combination of several factors, among which the size effect and surface state emission play much more important roles. A deep understanding of FL mechanism is vital to achieve desirable applications of CDs by regulating their particle size, surface states, doping elements, and so on.

4. Applications of L-w CDs

Different from the conventional QDs and commercial organic dyes, CDs hold numerous advantages such as convenient preparation, controllable surface functionalization, excellent photostability, superior biocompatibility, and valuable therapeutic functions. Apart from these features, L-w CDs also exhibit L-w emission and/or absorption property, which promotes their application in sensing (*in vitro* and *in vivo*) and cancer theranostics.

4.1. Sensing

Since surrounding environment has an obvious effect on the FL intensity of CDs, the emission quenching/enhancement of CDs could be induced by the ambient chemicals. Therefore, CDs can be developed as sensitive fluorescent probes for the qualitative and quantitative analysis of target substances. Among CD-based sensors, L-w CD-based probes exhibit unique advantages due to their large penetration depth and high signal-to-noise ratio. According to detection targets, L-w CD-based sensors can be classified into the following three types: 1) metal ion sensors [48,90-92], 2) biomolecular sensors [65,93-95], and 3) other sensors [96-98].

4.1.1. Metal ion sensors

We has fabricated a full-color emissive CDs (F-CD)-based multidimensional sensor array for the simultaneous detection and discrimination of diverse metal ions, including heavy, transitional, and

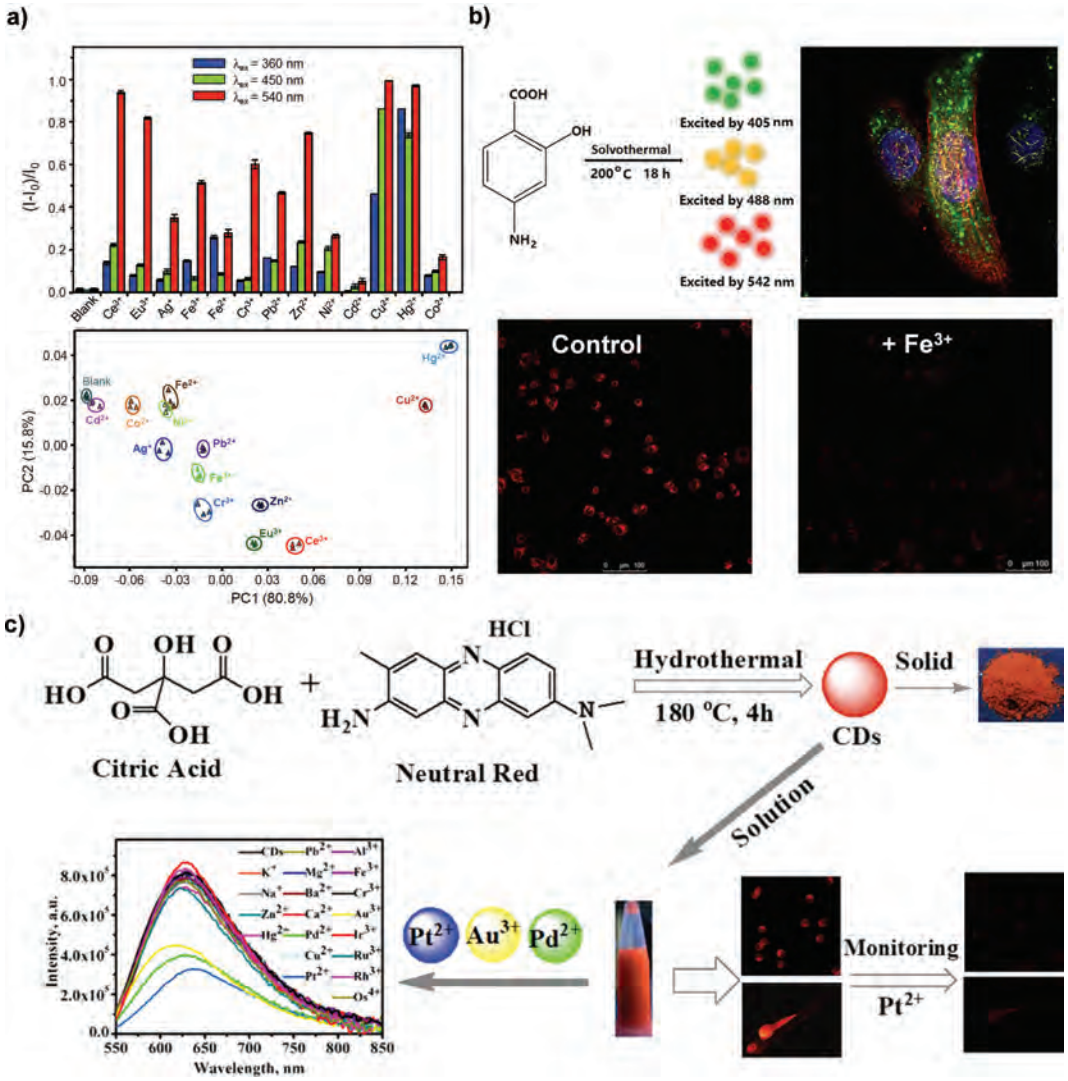

Fig. 4. (a) Three dominate emission maxima responses of F-CDs toward 13 metal ions and corresponding principal component analysis (PCA) plot for discrimination of a variety of metal ions. Reproduced with permission [48]. Copyright 2015, Wiley Publishing Group. (b) Preparation of color-tunable NCDs and their application in cell imaging and sensitive detection of Fe^{3+} in MCF-7 cells. Reproduced with permission [90]. Copyright 2017, American Chemical Society. (c) Synthesis of red emissive CDs for bioimaging and noble metal ions sensing both *in vitro* and *in vivo*. Reproduced with permission [92]. Copyright 2018, American Chemical Society.

rare-earth metal ions (Fig. 4a) [48]. Three dominant emission of F-CD were quenched in different degrees if encountered with various metal ions. Thus, by analyzing the FL variation among three emission channels, types of metal ions could be easily clarified. Song and co-workers also proposed a strategy to prepare FL sensors using color-adjustable N doped carbon dots (NCDs). Due to the superior optical property and favorable biocompatibility, NCDs have been used for cell imaging and Fe^{3+} sensing in living cells (Fig. 4b) [90]. A dynamic quenching mechanism has been proposed to explain the quenching phenomena induced by Fe^{3+} ions, where Fe^{3+} can coordinate with phenolic hydroxyl and amino groups on the surface of NCDs and consequently result in the transfer of excited electrons as well as enhanced nonradiative transition. Sun's group also reported that sensitive detection of Fe^{3+} could be achieved using S,N-doped CDs (S,N-CDs) probes [91]. The -COOH and thiocyanate (-SCN) on the surface of S,N-CDs could serve as active sites for the selective recognition of Fe^{3+} with detection limit of 9.7 mol/L. Moreover, the NIR emissive CDs with outstanding quantum yield of 33.96% were developed by Lu's group for selective Fe^{3+} sensing in living cells, which could also be used for the fabrication of light-emitting diodes [99]. To apply the L-w CDs sensors in a more complicated environment, Gao and co-workers synthesized red emissive CDs for noble metal ions detection (including Pt^{2+}, Au^{3+}, and Pd^{2+}) both i*n vitro* and *in vivo* (Fig. 4c) [92]. It was observed that FL intensity of the CDs gradually decreased along with the increase of Pt^{2+} concentration in zebrafish, which illustrated the feasibility of L-w CDs for metal ions detection in organisms.

4.1.2. Biomolecular sensors

Biomolecules play an indispensable role in flora and fauna, including signal transmission, phosphorylation, nutrition balance, physiological, and pathological processes [100]. Thus, it is quite significant to explore novel sensor systems for the sensitive detection of biomolecules, especially in complicated environments. By utilizing the specific optical properties, L-w CDs have been developed as fluorescent sensors for biomolecules detection both *in vitro* or *in vivo*, such as phosphate anions [93], peroxynitrite [94], ascorbic acid [101], and lysine [95].

Our group has fabricated a multi-channel fluorescent sensor array by utilizing ensembles of CDs and metal ions as sensing units for the discrimination of diverse phosphate anion (*i.e.*, ATP, ADP,

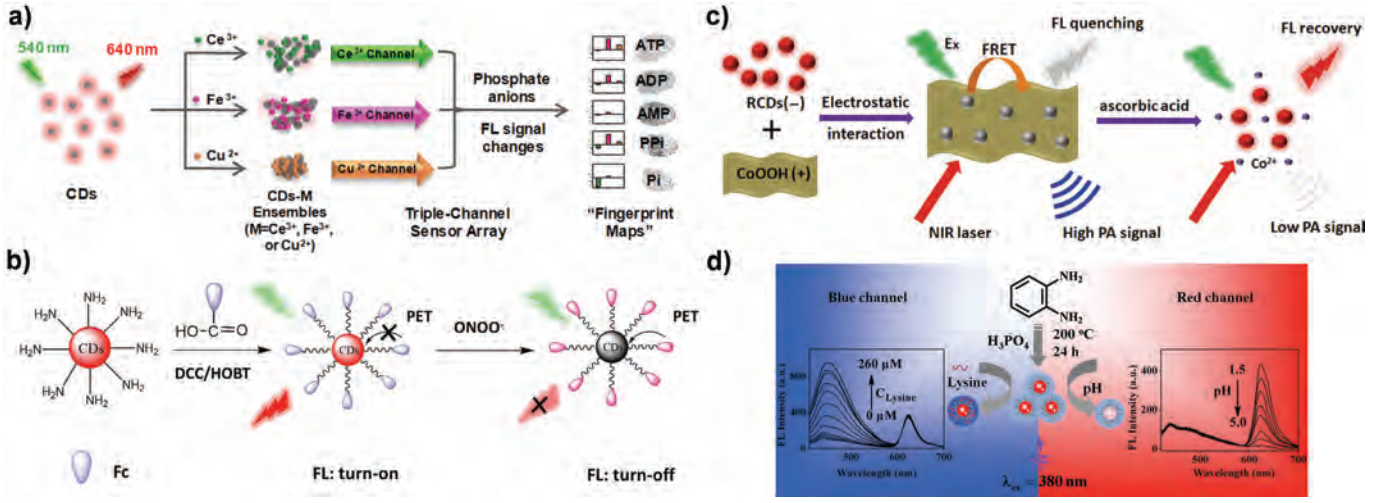

Fig. 5. Schematic Illustration of (a) the construction of CDs-based multichannel FL sensor array for the recognition and distinguish of phosphate anions. Reproduced with permission [93]. Copyright 2017, American Chemical Society. (b) The design and preparation of PET probe for $ONOO^-$ sensing. Reproduced with permission [94]. Copyright 2017, American Chemical Society. (c) The fabrication of RCDs-CoOOH nanoprobe for the detection of AA. Reproduced with permission [101]. Copyright 2018, Royal Society of Chemistry. (d) Preparation of CDs as dual emissive sensor for ratiometric detection of lysine and pH. Reproduced with permission [95]. Copyright 2017, American Chemical Society.

AMP, PPi, and Pi) (Fig. 5a) [93]. The FL of RCDs can be quenched differently by adding three kinds of metal ions (*i.e.*, Ce^{3+}, Fe^{3+}, and Cu^{2+}). Interestingly, the diverse phosphate anions lead to the recovery or further quenching of FL due to the further disaggregation or aggregation of CD-metal ion ensembles. Therefore, phosphate anions can be successfully recognized according to the FL variation of CDs. Subsequently, we designed a photo-induced electron transfer (PET) probe for peroxynitrite ($ONOO^-$) detection based on ferrocene (Fc)-modified CDs (Fig. 5b) [94]. The electron transfer from Fc to CDs is largely promoted by the introduction of $ONOO^-$ due to the lowered HOMO of CDs, which could lead to an obvious FL quenching. Owing to the excellent biocompatibility, nanoprobe can be utilized for intracellular $ONOO^-$ sensing. To further expand the applicable range of L-w CD-based probes, our group fabricated a bifunctional probe for ascorbic acid (AA) sensing in biological systems (Fig. 5c) [65]. RCDs and cobalt oxyhydroxide (CoOOH) were selected as FL and PA responsive units, respectively. Due to the FL resonance energy transfer (FRET) between RCDs and CoOOH, the FL signal of composite probe was kept at "off" state, while the PA performance was preserved. When encountering AA, CoOOH was reduced to Co^{2+} and accompanied with the release of RCDs, leading to diminished PA signal as well as recovered FL emission. In addition, our group also developed CD-based sensors for the detection of other biomolecules such as cysteine [65], hypochlorite [102], dopamine [103] and glutathione [104], which exhibited satisfactory sensing results, specifically in physiological environment. To further improve the detection accuracy and reduce the interference that caused by environmental variation and excitation source fluctuation, Song and co-workers developed dual emissive nanoprobe based on functional CDs for the ratiometric detection of both lysine and pH at cellular level (Fig. 5d) [95]. Under the excitation of 380 nm light, the as-prepared CDs displayed two characteristic emission peaks at around 440 and 624 nm, which were particularly sensitive to lysine and pH, respectively. The dual emissive property, low cytotoxicity, and favorable colloidal stability make these CDs to be promising candidate for the ratiometric detection in cellular system. Moreover, to achieve the sensing of specific biomolecular in deep tissues, two-photon fluorescent probe was developed by Wang and co-workers based on red emissive CDs for the detection of formaldehyde in living cells and zebrafishes. This nanoprobe exhibited rapid response, favorable sensitivity, outstanding selectivity and deep tissue penetration capacity as high as 240 μm [105].

4.1.3. Other sensors

Apart from the metal ions and biomolecules, L-w CD-based sensors have also been utilized for the detection of drugs, vapor, and biomarkers by exploring the FL variation between "on" and "off" states. Our group has constructed an antibiotic sensing platform based on the ensembles of full-color emissive CDs (F-CDs) and screened metal ions [96]. Multi emissive channel of F-CDs with different quenching degrees are used as various sensing units. In the presence of different antibiotics, FL restoration or further quenching of F-CDs appears due to the competition of metal ions between F-CDs and antibiotics, leading to distinguishable FL responsive signals. By using standard statistical methods, the multi-channel sensing platform can be applied for the differentiation of antibiotics in real food samples. For early diagnosis of lung cancer, Pan's group designed a NIR emissive CDs-based aptasensor for the specific recognition of carcinoembryonic antigen (CEA, a biomarker of tumors) in pleural effusion [97]. DNA-modified NIR CDs and SiO_2-coated gold nanorods (AuNRs) that decorated with aptamer were used as building blocks for the construction of nanosensor. By FRET effect between AuNRs and NIR CDs, the as-fabricated probe was kept at quenched state, and the FL emission would be activated only in the presence of CEA due to the specific combination between CEA and decorated aptamer. This nanosensor displayed satisfactory CEA recognition capacities especially in real pleural effusion samples. Solid-state sensors constructed with L-w CDs have also been developed for vapor detection. Liang's group fabricated a gaseous ammonia probing platform by coating RCDs onto polyvinylidene fluoride membrane [98]. Noxious gaseous ammonia could be sensitively and specifically detected within tens of seconds using the solid-state FL sensor. Besides, the responsive mechanism was further analyzed, *i.e.*, the deprotonation of carboxyl groups and Michael addition reaction of unsaturated groups were mainly responsible for the quenching of CDs FL in the presence of ammonia gas.

4.2. Cancer theranostics

Theranostics, which finely integrates diagnostic imaging functions (*e.g.*, ultrasonography, magnetic resonance imaging (MRI), positron emission tomography (PET), FL, and PA imaging) and therapeutic modalities (*e.g.*, chemotherapy, radiotherapy, immunotherapy, and phototherapy), not only improves the therapeutic efficacy

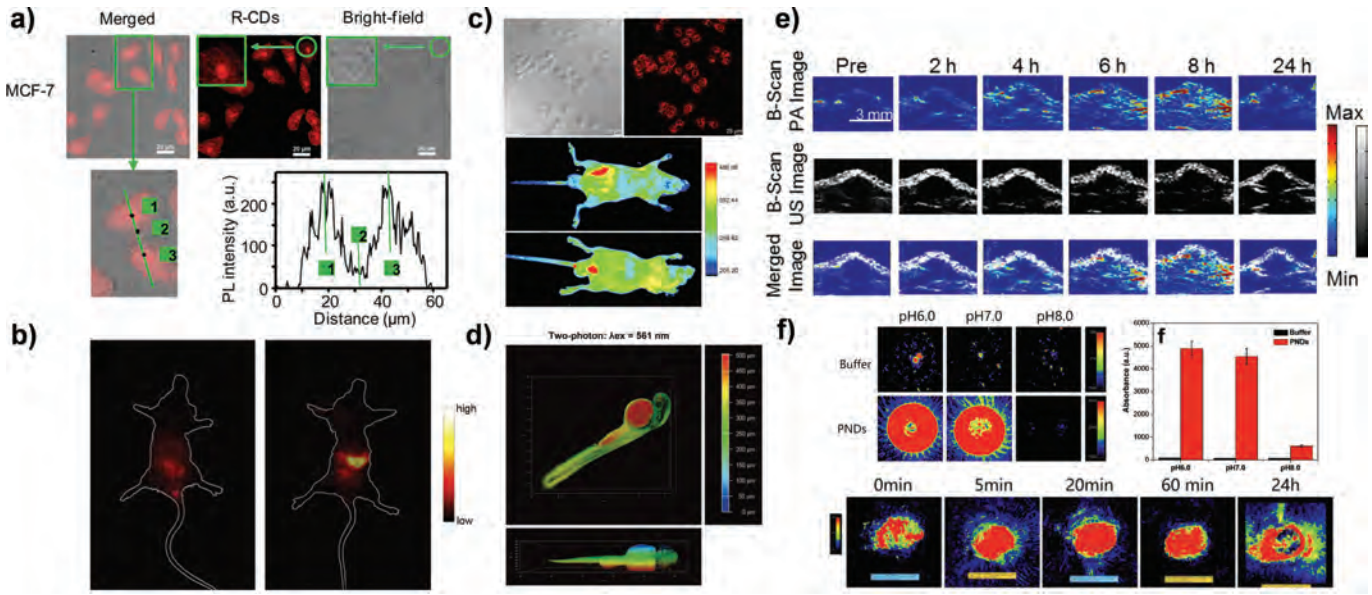

Fig. 6. (a) Nucleolus targeted FL images of RCDs among MCF-7 cells and corresponding quantitative results. Reproduced with permission [39]. Copyright 2016, American Chemical Society. (b) Stomach FL images of living mouse with and without the gavage injection of CDs/PVP. Reproduced with permission [71]. Copyright 2018, Wiley Publishing Group. (c) FL images of HeLa cells and nude mouse after incubation and subcutaneous injection with NIR emissive CDs, respectively. Reproduced with permission [107]. Copyright 2019, Elsevier. (d) Two photon FL images of zebrafish larvae cultured with T-CQDs. Reproduced with permission [109]. Copyright 2019, Royal Society of Chemistry. (e) PA and ultrasound images of tumor section in living mouse after intravenous (i.v.) injection of modified CDs. Reproduced with permission [32]. Copyright 2019, American Chemical Society. (f) PA images of PNDs dispersed in various pH buffer and intratumorally injected into tumor area after conjugated with Cetuximab. Reproduced with permission [112]. Copyright 2018, American Chemical Society.

but also spurs the development of personalized medicine [106]. Among various nanomaterial-based theranostic platforms, L-w CDs are regarded as a powerful candidate for biological applications due to their favorable biocompatibility, superior stability, broad absorption range, limited photodamage, and most importantly large tissue penetration capacity and treatment potentials, which enable real-time imaging and non-invasive therapy.

4.2.1. Bioimaging

Benefiting from their attractive optical properties, L-w CDs have been developed as multifunctional bioimaging probes. For instance, our group reported efficient RCDs that could serve as nucleolus-targeted imaging agent. It has been found that nucleoli of cancer cells could be specifically lighted up by the bright red light emitted from CDs (Fig. 6a) [39]. The observed nucleoli-selective imaging capacity of RCDs was resulted from spatial accumulation instead of their interaction with RNA. Li and co-workers synthesized poly(vinylpyrrolidone) (PVP)-decorated NIR emissive CDs that were capable of stomach imaging of living mice [71]. Intense luminescence signal was observed in mouse stomach under safety laser irradiation power after gavage injection of CDs/PVP (Fig. 6b). This work illustrated the great potential of surface-engineered CDs in bioimaging. Ding's group also designed NIR-emissive CDs for both *in vitro* and *in vivo* bioimaging by using lemon juice (a renewable and green resource) as precursor (Fig. 6c) [107]. The outstanding water solubility, L-w emissive property (λ = 704 nm), and high QY (31%) made the as-prepared CDs become a valuable imaging agent in physiological environment.

Besides, motivated by the minimized photodamage, enlarged tissue penetration depth and the lowered auto-fluorescence, CDs with multiphoton excited L-w emissive capacity were further applied for bioimaging. For example, Lu and co-workers reported the polymer–carbon nanodots with both L-w emissive (centered at around 710 nm) and two-photon FL properties. Their feasibility for *in vivo* bioimaging was confirmed as well [108]. Jia's group proposed a novel strategy for the preparation of red emissive CDs (named T-CQDs) with narrow FWHM [109]. The T-CQDs displayed excellent imaging performance in zebrafish larva under one-photon or two-photon excitation modes, and the penetration depth of T-CQDs could reach to ~500 μm (Fig. 6d). Multiphoton (including 2, 3 and 4 photon) excited upconversion L-w emissive CDs were developed by Liu and coworkers *via* the *in-situ* solvent-free approach. The superior imaging capacity was demonstrated by their two-photon FL imaging performance toward murine melanoma cells under the excitation of 800 nm [110].

PA imaging is a novel non-invasive imaging technique, which provides high-resolution and ultra-sensitive imaging results in deep tissue by integrating the superior selectivity of laser light and large diffusive domains of ultrasound [111]. L-w CDs, especially those with broad absorption band tail up to the NIR region, have garnered significant attention as PA imaging agents. We synthesized photosensitizer modified RCDs with favorable PA imaging ability [32]. PA and ultrasound dual-modal imaging results illustrated the feasibility of utilizing CDs for PA imaging with satisfactory contrast (Fig. 6e). Wu and co-workers designed porphyrin-implanted CDs (PNDs) with solvent-dependent NIR emission and absorption, which were successfully applied for FL and PA imaging [112]. The PA response of PNDs was further confirmed through intratumoral imaging results (Fig. 6f).

4.2.2. Phototherapy

Several studies have revealed that the therapeutic potentials of L-w CDs, specifically the generation of hyperthermia and ROS under laser irradiation, which enable applications in photothermal therapy (PTT) and photodynamic therapy (PDT). Hao's group reported that the NIR-II-emissive CDs (NIR II CDs) that were synthesized from watermelon can serve as efficient photothermal agent (Fig. 7a) [113]. Activated by 808 nm laser, they not only exhibited favorably NIR-II-emission property but also excellent photothermal performance with high photon-thermal conversion efficiency of 30.6%, demonstrating their advantages in bioimaging and thermal ablation of tumor. To enhance the therapeutic effi-

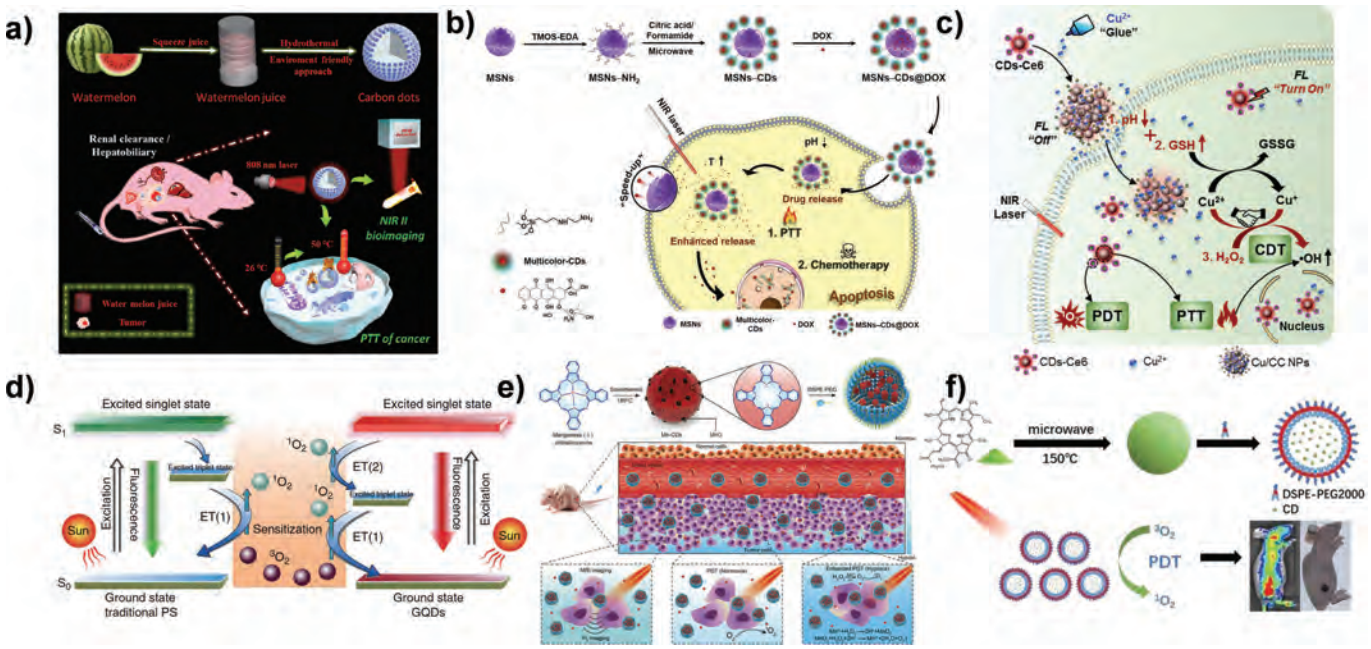

Fig. 7. Schematic diagram of (a) preparation of NIR II CDs for bioimaging and thermal ablation of tumor. Reproduced with permission [113]. Copyright 2019, American Chemical Society. (b) Synthetic route of MSNs-CDs@DOX and the application in multicolor FL imaging guided PTT combined chemotherapy. Reproduced with permission [114]. Copyright 2020, Wiley Publishing Group. (c) Synthesis of Cu/CC NPs and for TEM stimuli-responsive FL imaging and synergistic therapy. Reproduced with permission [115]. Copyright 2020, Wiley Publishing Group. (d) Conventional (left) and multistate (right) photosensitization process. Reproduced with permission [116]. Copyright 2014, Nature. (e) Fabrication of Mn-CD assembly as *in-situ* oxygen-supplied theranostic platform for enhanced PDT. Reproduced with permission [117]. Copyright 2018, Wiley Publishing Group. (f) Synthesis of pheophytins-derived CDs for FL imaging and PDT-contained synergistic therapy. Reproduced with permission [118]. Copyright 2019, Wiley Publishing Group.

cacy and diminish potential adverse effects, L-w CD-based PTT was also collaborated with other treatment modes, such as chemotherapy, PDT, and chemodynamic therapy (CDT). Our group has fabricated CDs-mesoporous silica nanohybrids (MSNs-CDs), which combines multicolor-emitting property, photothermal function, and drug loading capacity into one therapeutic platform (Fig. 7b) [114]. Compared to single therapeutic mode, MSNs-CDs loaded with doxorubicin (DOX, a typical anti-tumor drug) are endowed with PTT and chemotherapy effects, which provide extremely high therapeutic efficiency due to the accelerated release of DOX induced by photothermal effects. In addition, our group designed intelligent tumor microenvironment (TME) stimuli-responsive nanoconstruction assembled from chlorine e6 (Ce6)-conjugated CDs and copper ions (named Cu/CC NPs) for FL imaging-guided synergistic therapy (Fig. 7c) [115]. Ce6-decorated RCDs (CDs-Ce6) facilitated deep-tissue imaging and synergetic PTT and PDT effects, meanwhile copper ions could act as chelate center as well as CDT agent. Notably, the FL imaging, CDT, and PDT abilities of as-fabricated nanoassemblies could only be triggered in TME due to the influence of mild acidic condition, overexpressed hydrogen peroxide (H_2O_2) and glutathione (GSH), and thus the amplified treatment efficiency could be achieved with minimized side effects.

Different from endowing the L-w CD-based theranostic platform with PDT function through modification of organic PDT agents, the intrinsic ROS generation ability of CDs under laser irradiation provides several attractive advantages, such as favorable water solubility, high photostability, and adjustable absorption characteristics. Through ingenious design of precursors, Ge and co-workers developed deep-red emissive GQDs as an efficient PDT agent with high singlet oxygen ($^1O_2$) production yield up to 1.3 [116]. The surprising $^1O_2$ generation capacity of GQDs is stemmed from the multistate photosensitization (Fig. 7d). The satisfactory PDT efficacy of GQDs was verified both *in vitro* and *in vivo*, which illustrated that CDs can be used as a promising nano-photosensitizer for phototherapy. Since the CDs sensitize the ground state triplet oxygen to generate $^1O_2$ as ROS, their therapeutic efficacy is limited by the amount of oxygen in hypoxic TME. Wang's group further designed an *in-situ* oxygen-supplied theranostic platform by assembling Mn-doped CDs and DSPE-PEG (Fig. 7e) [117]. The Mn-CD nano-assemblies served as a smart contrast agent for both NIR FL and T_1-weighted magnetic resonance imaging. Most importantly, Mn-CD assembly could catalyze the endogenous H_2O_2 to generate oxygen, which helped to alleviate the tumor hypoxia and subsequently enhanced the PDT efficacy. This study might lead to a new generation of CD-related nanoagents for TME-adaptable photodynamic treatment. Afterward, Wang's group explored natural biomass as a carbon source for the facile synthesis of CDs with photosensitization ability (Fig. 7f) [118]. The as-prepared CDs exhibited obvious NIR FL emission and high $^1O_2$ production yield, suggesting the great application potential of pheophytin-derived CDs as multifunctional PDT agent.

Overall, the unique two-photon excited FL emission, broad absorption band, sensitive PA response, convenient surface modification, and photo-mediated treatment functions make L-w CDs to be promising theranostic agents, which hold great potential in bioimaging-assisted diagnosis and TME stimuli-responsive synergistic therapy.

5. Summary and perspectives

Owing to the unique advantages in biosensing, deep tissue imaging, photo-triggered therapy, photocatalysis, and optoelectronic devices, L-w CDs have attracted lots of attention in recent years and been regarded as a "rising star" among luminescent nanomaterials. In this review, we summarized the intriguing aspects and research progresses of L-w CDs. Firstly, the crucial factors for the synthesis of L-w CDs, including precursors, reaction conditions, and post modification routes, were reviewed to support their rational design. In particularly, we focused on the FL mechanism of L-w CDs, which played a key role in realizing specific ap-

plications through regulating particle size, surface states, and doping elements. Then, applications of L-w CDs in sensing and cancer theranostics (including bioimaging and photo-mediated treatments) were highlighted. These applications are supported by the fascinating merits of CDs such as red-shifted emission and excitation, two-photon excited emission, PA response, easy surface modification, and photo-activated heat and/or ROS generation. However, further studies and improvements are still required to expand the practical applications of L-w CDs. The current challenges and future perspectives are stated as follows:

1) The red or NIR FL emission of most reported CDs are less-desirable and commonly suffer from low QY. Exploring new strategies to synthesize CDs with L-w emissive property and high QY is indispensable. In addition, the large-scale preparation of L-w CDs with stable characteristics remains a crucial challenge. Thus, reproducible synthesis of L-w CDs from green, especially biomass precursors *via* time and energy saving approaches is urgently required.
2) Although several theories have been proposed to clarify the FL mechanism of L-w CDs, a comprehensive understanding is still lacking. Therefore, advanced characterization techniques such as lifetime microscopy, scanning tunneling microscopy, single-particle imaging and emission, and relevant super-resolution techniques, as well as the effective simulation methods including the theoretical calculation and computational modeling (such as machine learning) are highly desired to elucidate the FL mechanism of L-w CDs.
3) L-w CDs hold great potential in biomedical applications, especially in biosensors and cancer theranostics. However, their practical applications are severely hindered by the safety concern such as long-term toxicity. Further studies are required to focus on their biodistribution, pharmacokinetics, and clearance.

Overall, although great progresses have been made in both fundamental understanding and practical application of L-w CDs, several issues still need to be resolved. Through integrating theoretical and experimental explorations, L-w CDs are expected to play a much more important role in extensive fields.

Declaration of competing interest

The authors declare that they have no known competing financial interests or personal relationships that could have appeared to influence the work reported in this paper.

Acknowledgments

The authors acknowledge the financial support from the National Natural Science Foundation of China (Nos. 51902323, 51872300 and U1832110), Postdoctoral Science Foundation of China (No. 2020M671831), S&T Innovation 2025 Major Special Program of Ningbo (No. 2018B10054), Zhejiang Provincial Natural Science Foundation of China (No. LY20B050003).

References

[1] V. Georgakilas, J.A. Perman, J. Tucek, R. Zboril, Chem. Rev. 115 (2015) 4744–4822.
[2] S. Zhu, Y. Song, X. Zhao, et al., Nano Res. 8 (2015) 355–381.
[3] J.J. Liu, R. Li, B. Yang, ACS Central Sci. 6 (2020) 2179–2195.
[4] X. Xu, R. Ray, Y. Gu, et al., J. Am. Chem. Soc. 126 (2004) 12736–12737.
[5] H. Li, Z. Kang, Y. Liu, S.T. Lee, J. Mater. Chem. 22 (2012) 24230–24253.
[6] Y. Wu, Q. Li, D. Yang, J. Liao, Nanosci. Nanotechnol. Lett. 9 (2017) 1827–1848.
[7] B. Lyu, H.J. Li, F. Xue, et al., Chem. Eng. J. 388 (2020) 124285.
[8] S.C. Ray, A. Saha, N.R. Jana, R. Sarkar, J. Phys. Chem. C 113 (2009) 18546–18551.
[9] H. Zhu, X. Wang, Y. Li, et al., Chem. Commun. (2009) 5118–5120.
[10] J. Zhou, C. Booker, R. Li, et al., J. Am. Chem. Soc. 129 (2007) 744–745.
[11] Q.L. Zhao, Z.L. Zhang, B.H. Huang, et al., Chem. Commun. (2008) 5116–5118.
[12] S.L. Hu, K.Y. Niu, J. Sun, et al., J. Mater. Chem. 19 (2009) 484–488.
[13] X. Li, H. Wang, Y. Shimizu, et al., Chem. Commun. 46 (2010) 932–934.
[14] S. Anwar, H. Ding, M. Xu, et al., ACS Appl. Bio. Mater. 2 (2019) 2317–2338.
[15] B. Yao, H. Huang, Y. Liu, Z. Kang, Trends Chem 1 (2019) 235–246.
[16] Y. Yan, J. Gong, J. Chen, et al., Adv. Mater. 21 (2019) 1808283.
[17] B.B. Chen, M.L. Liu, C.M. Li, C.Z. Huang, Adv. Colloid Interface Sci. 270 (2019) 165–190.
[18] M. Shamsipur, A. Barati, S. Karami, Carbon 124 (2017) 429–472.
[19] M.J. Molaei, Anal. Methods 12 (2020) 1266–1287.
[20] Y. Choi, X.T. Zheng, Y.N. Tan, Mol. Syst. Des. Eng. 5 (2020) 67–90.
[21] S. Miao, K. Liang, J. Zhu, et al., Nano Today 33 (2020) 100879.
[22] B. Li, S. Zhao, L. Huang, et al., Chem. Eng. J. 408 (2021) 127245.
[23] W.D. Li, Y. Liu, B.Y. Wang, et al., Chin. Chem. Lett. 30 (2019) 2323–2327.
[24] H. Ding, X.X. Zhou, J.S. Wei, et al., Carbon 167 (2020) 322–344.
[25] D. Gao, H. Zhao, X. Chen, H. Fan, Mater. Today Chem. 9 (2018) 103–113.
[26] S. Qu, D. Zhou, D. Li, et al., Adv. Mater. 28 (2016) 3516–3521.
[27] Y. Wu, H. Zhang, A. Pan, et al., Adv. Sci. 6 (2019) 1801432.
[28] H.Q. Song, X.J. Liu, B.Y. Wang, Z.Y. Tang, S.Y. Lu, Sci. Bull. 64 (2019) 1788–1794.
[29] P.G. Luo, S. Sahu, S.T. Yang, et al., J. Mater. Chem. B 1 (2013) 2116–2127.
[30] Y. Liu, Q. Jia, J. Zhou, Adv. Ther. 1 (2018) 1800055.
[31] L. Jiang, H. Ding, M. Xu, et al., Small 19 (2020) 2000680.
[32] S. Sun, J. Chen, K. Jiang, et al., ACS Appl. Mater. Interfaces 11 (2019) 5791–5803.
[33] M. Hassan, V.G. Gomes, A. Dehghani, S.M. Ardekani, Nano Res. 1 (2018) 1–41.
[34] Y.P. Sun, B. Zhou, Y. Lin, et al., J. Am. Chem. Soc. 128 (2006) 7756–7757.
[35] L. Cao, X. Wang, M.J. Meziani, et al., J. Am. Chem. Soc. 129 (2007) 11318.
[36] H. Liu, T. Ye, C. Mao, Angew. Chem. Int. Ed. 46 (2007) 6473–6475.
[37] J. Peng, W. Gao, B.K. Gupta, et al., Nano Lett. 12 (2012) 844–849.
[38] Z.C. Yang, M. Wang, A.M. Yong, et al., Chem. Commun. 47 (2011) 11615–11617.
[39] S. Sun, L. Zhang, K. Jiang, A. Wu, H. Lin, Chem. Mater. 28 (2016) 8659–8668.
[40] X. Zhai, P. Zhang, C. Liu, et al., Chem. Commun. 48 (2012) 7955–7957.
[41] S. Qu, X. Wang, Q. Lu, X. Liu, L. Wang, Angew. Chem. Int. Ed. 51 (2012) 12215–12218.
[42] L. Pan, S. Sun, L. Zhang, K. Jiang, H. Lin, Nanoscale 8 (2016) 17350–17356.
[43] J. Ge, Q. Jia, W. Liu, et al., Adv. Mater. 27 (2015) 4169–4177.
[44] S. Li, W. Su, H. Wu, et al., Nat. Biomed. Eng. 4 (2020) 704–716.
[45] M. Zheng, Y. Li, S. Liu, et al., ACS Appl. Mater. Interfaces 8 (2016) 23533–23541.
[46] J. Liu, Y. Geng, D. Li, et al., Adv. Mater. 32 (2020) 1906641.
[47] L. Li, R. Zhang, C. Lu, et al., J. Mater. Chem. B 5 (2017) 7328–7334.
[48] L. Pan, S. Sun, A. Zhang, et al., Adv. Mater. 27 (2016) 7782–7787.
[49] D. Huang, H. Zhou, Y. Wu, et al., Carbon 142 (2019) 673–684.
[50] Z. Tian, X. Zhang, D. Li, et al., Adv. Opt. Mater. 5 (2017) 1700416.
[51] L. Wang, W. Li, L. Yin, et al., Sci. Adv. 40 (2020) eabb6772.
[52] H. Tetsuka, A. Nagoya, T. Fukusumi, T. Matsui, Adv. Mater. 28 (2016) 4632–4638.
[53] M. Zheng, L. Qiao, Y. Su, P. Gao, Z. Xie, J. Mater. Chem. B 7 (2019) 3840–3845.
[54] B.Y. Wang, J.K. Yu, L.Z. Sui, et al., Adv. Sci. 8 (2021) 2001453.
[55] F. Yuan, Z. Wang, X. Li, et al., Adv. Mater. 3 (2016) 1604436.
[56] K. Jiang, S. Sun, L. Zhang, et al., Angew. Chem. Int. Ed. 54 (2015) 5360–5363.
[57] C.C. Ke, Y.C. Yang, W.L. Tseng, Part. Part. Syst. Charact. 33 (2016) 132–139.
[58] J. Zhu, X. Bai, X. Chen, et al., Adv. Opt. Mater. 7 (2019) 1801599.
[59] Z. Zhu, Y. Zhai, Z. Li, et al., Mater. Today 30 (2019) 52–79.
[60] S. Hu, A. Trinchi, P. Atkin, I. Cole, Angew. Chem. Int. Ed. 54 (2015) 2970–2974.
[61] K. Jiang, X. Feng, X. Gao, et al., Nanomaterials 4 (2019) 529.
[62] H. Ding, S.B. Yu, J.S. Wei, H.M. Xiong, ACS Nano 10 (2016) 484–491.
[63] H.A. Nguyen, I. Srivastava, D. Pan, M. Gruebele, ACS Nano 14 (2020) 6127–6137.
[64] L. Jiang, H.H. Ding, M.S. Xu, et al., Small 16 (2020) 9.
[65] K. Jiang, S. Sun, L. Zhang, et al., ACS Appl. Mater. Interfaces 7 (2015) 23231–23238.
[66] M. Lan, S. Zhao, Z. Zhang, et al., Nano Res 10 (2017) 3113–3123.
[67] Y. Liu, W. Duan, W. Song, et al., ACS Appl. Mater. Interfaces 9 (2017) 12663–12672.
[68] S. Khan, A. Gupta, N.C. Verma, C.K. Nandi, Nano Lett 15 (2015) 8300–8305.
[69] T. Zhang, J. Zhu, Y. Zhai, et al., Nanoscale 9 (2017) 13042–13051.
[70] H. Wang, C. Sun, X. Chen, et al., Nanoscale 9 (2017) 1909–1915.
[71] D. Li, P. Jing, L. Sun, et al., Adv. Mater. 13 (2018) 1705913.
[72] F. Yuan, Z. Wang, X. Li, et al., Adv. Mater. 29 (2017) 1604436.
[73] R. Ye, C. Xiang, J. Lin, et al., Nat. Commun. 4 (2013) 2943.
[74] J.S. Donner, S.A. Thompson, M.P. Kreuzer, G. Baffou, R. Quidant, Nano Lett 12 (2012) 2107–2111.
[75] Y. Dong, C. Chen, X. Zheng, et al., J. Mater. Chem. 22 (2012) 8764–8766.
[76] S. Qu, D. Zhou, D. Li, et al., Adv. Mater. 28 (2016) 3516–3521.
[77] Z. Tian, X. Zhang, D. Li, et al., Adv. Opt. Mater. 5 (2017) 1700416.
[78] L. Bao, C. Liu, Z.L. Zhang, D.W. Pang, Adv. Mater. 27 (2015) 1663–1667.
[79] S. Tao, S. Zhu, T. Feng, et al., Mater. Today Chem. 6 (2017) 13–25.
[80] J. Fan, P.K. Chu, Small 6 (2010) 2080–2098.
[81] K. Hola, M. Sudolska, S. Kalytchuk, et al., ACS Nano 11 (2017) 12402–12410.
[82] M. Lan, L. Guo, S. Zhao, et al., Adv. Ther. 1 (2018) 1800077.
[83] S. Yang, J. Sun, X. Li, et al., J. Mater. Chem. A 2 (2014) 8660–8667.
[84] O. Kozák, M. Sudolská, G. Pramanik, et al., Chem. Mater. 28 (2016) 4085–4128.
[85] M. Wu, Y. Wang, W. Wu, et al., Carbon 78 (2014) 480–489.
[86] L. Li, B. Yu, T. You, Biosens. Bioelectron. 74 (2015) 263–269.
[87] J.H. Jou, Y.X. Lin, S.H. Peng, et al., Adv. Funct. Mater. 24 (2014) 555–562.

[88] S. Shao, J. Ding, L. Wang, X. Jing, F. Wang, J. Am. Chem. Soc. 134 (2012) 20290–20293.
[89] N. Mataga, Y. Kaifu, M. Koizumi, Bull. Chem. Soc. Jpn. 29 (1956) 465–470.
[90] Y. Song, C. Zhu, J. Song, et al., ACS Appl. Mater. Interfaces 9 (2017) 7399–7405.
[91] X. Miao, X. Yan, D. Qu, et al., ACS Appl. Mater. Interfaces 9 (2017) 18549–18556.
[92] W. Gao, H. Song, X. Wang, et al., ACS Appl. Mater. Interfaces 10 (2018) 1147–1154.
[93] S. Sun, K. Jiang, S. Qian, Y. Wang, H. Lin, Anal. Chem. 89 (2017) 5542–5548.
[94] J. Zhu, S. Sun, K. Jiang, et al., Biosens. Bioelectron. 97 (2017) 150–156.
[95] W. Song, W. Duan, Y. Liu, et al., Anal. Chem. 24 (2017) 13626–13633.
[96] L.N. Qiao, S. Qian, Y. Wang, S. Yan, H. Lin, Chem. Eur. J. 24 (2018) 4703–4709.
[97] K. Shao, L. Wang, Y. Wen, et al., Anal. Chim. Acta 1068 (2019) 52–59.
[98] B.P. Jiang, B. Zhou, X.C. Shen, et al., Chem. Eur. J. 21 (2015) 18993–18999.
[99] B.Y. Wang, J. Li, Z.Y. Tang, B. Yang, S.Y. Lu, Sci. Bull. 64 (2019) 1285–1292.
[100] S.H. Miao, K. Liang, B. Kong, Mat. Chem. Front. 4 (2020) 128–139.
[101] W. Xu, J. Chen, S. Sun, et al., Nanoscale 10 (2018) 17834–17841.
[102] L. Ma, S. Sun, Y. Wang, et al., Microchim. Acta 184 (2017) 3833–3840.
[103] Z.D. Tang, K. Jiang, S. Sun, et al., Analyst 144 (2019) 468–473.
[104] J. Li, Y. Wang, S. Sun, et al., Analyst 145 (2020) 2982–2987.
[105] H. Wang, J. Wei, C.H. Zhang, et al., Chin. Chem. Lett. 31 (2020) 759–763.
[106] Z. Peng, X. Han, S. Li, A.O. Al-Youbi, et al., Coord. Chem. Rev. 343 (2017) 256–277.
[107] H. Ding, X. Zhou, B. Qin, Z. Zhou, Y. Zhao, J. Lumin. 211 (2019) 298–304.
[108] S.Y. Lu, L.Z. Sui, J.J. Liu, et al., Adv. Mater. 29 (2017) 1603443.
[109] Y. Liu, H. Gou, X. Huang, et al., Nanoscale 12 (2020) 1589–1601.
[110] K.K. Liu, S.Y. Song, L.Z. Sui, et al., Adv. Sci. 6 (2019) 1900766.
[111] C. Lee, W. Kwon, S. Beack, et al., Theranostics 6 (2016) 2196–2208.
[112] F. Wu, H. Su, Y. Cai, et al., ACS Appl. Bio Mater. 1 (2018) 110–117.
[113] Y. Li, G. Bait, S. Zeng, J. Hao, ACS Appl. Mater. Interfaces 11 (2019) 4737–4744.
[114] S. Sun, S. Zhao, K. Jiang, et al., ChemNanoMat 6 (2020) 953–962.
[115] S. Sun, Q. Chen, Z. Tang, et al., Angew. Chem. Int. Ed. 59 (2020) 21041–21048.
[116] J. Ge, M. Lan, B. Zhou, et al., Nat. Commun. 5 (2014) 4596.
[117] Q. Jia, J. Ge, W. Liu, et al., Adv. Mater. 30 (2018) 1706090.
[118] Y. Wen, Q. Jia, F. Nan, et al., Chem. Asian J. 14 (2019) 2162–2168.